

Skill-informed Data-driven Haptic Nudges for High-dimensional Human Motor Learning

Ankur Kamboj¹, Rajiv Ranganathan², Xiaobo Tan¹, and Vaibhav Srivastava¹ *

Abstract

In this work, we propose a data-driven skill-informed framework to design optimal haptic nudge feedback for high-dimensional novel motor learning tasks. We first model the stochastic dynamics of human motor learning using an Input-Output Hidden Markov Model (IOHMM), which explicitly decouples latent skill evolution from observable kinematic emissions. Leveraging this predictive model, we formulate the haptic nudge feedback design problem as a Partially Observable Markov Decision Process (POMDP). This allows us to derive an optimal nudging policy that minimizes long-term performance cost, implicitly guiding the learner toward robust regions of the skill space. We validated our approach through a human-subject study ($N = 30$) using a high-dimensional hand-exoskeleton task. Results demonstrate that participants trained with the POMDP-derived policy exhibited significantly accelerated task performance compared to groups receiving heuristic-based feedback or no feedback. Furthermore, synergy analysis revealed that the POMDP group discovered efficient low-dimensional motor representations more rapidly.

1 Introduction

The integration of robotic systems into human spaces presents a transformative opportunity to improve humans’ quality of life through automated and personalized physical assistance during skill acquisition and motor rehabilitation. Haptic feedback has proven to be a powerful modality to guide human motor motions, thus improving task performance and skill learning without fostering dependence on robotic assistance [1, 2]. However, learning to perform high-dimensional *de-novo* (novel) tasks, like using a tool or recovering motor function post neurological injury, is much harder than simple low-dimensional reaching movements [3]. Consequently, designing haptic assistance for such complex tasks is an open challenge since determining the optimal/perfect movement for such tasks is non-trivial; *de-novo* learning involves discovering a movement strategy, rather than simply reducing task error.

Haptic guidance designs for physical human robot interaction regimes can be broadly categorized into two approaches: using expert-guidance or based on observed task performance metrics. The first category involves field experts and professionals designing haptic guidance systems informed by their intuition, experience, and knowledge [4–6]. This “top-down” approach is not suitable for high degrees of freedom (DoF) tasks where the solution space is vast, owing to redundancy in motor space, and finding optimal motions to instruct the right motor coordination strategies is non-trivial [7]. The second category exploits directly observable task performance metrics like task errors, movement time, smoothness, or task success [8–11]. While this reactive strategy is intuitive and easy to design, it can often be misleading as performance is a noisy measure of true skill, especially for high DoF tasks. The assistance design might overfit to the user, helping them perform well temporarily (low errors) by using a bad, compensatory habit (low skill). The simplified task

*This work was supported by NSF Grant CMMI-1940950.

¹A. Kamboj (ankurank@msu.edu), X. Tan (xbtan@msu.edu), and V. Srivastava (vaibhav@msu.edu) are with the Department of Electrical and Computer Engineering, Michigan State University, USA.

²R. Ranganathan (rrangana@msu.edu) is with the Department of Kinesiology and the Department of Mechanical Engineering, Michigan State University, USA.

performance might not capture important features of the underlying latent skill state, thus leading learners toward suboptimal solutions. This prevents mastery of high-dimensional skill and ultimately hinders long-term skill development.

To address these limitations, we propose haptic assistance designs informed by latent skill rather than task performance corrections. Central to our approach is the recognition that motor learning is a latent process, where observable kinematic performance is a noisy emission of the underlying evolving cognitive control strategy [12]. Drawing on cognitive diagnosis and human skill modeling literature [12–15], we formalize motor learning as a progression through discrete latent states, paralleling the cognitive, associative, and autonomous phases proposed by Fitts and Posner [16]. While standard Hidden Markov Models (HMM) have successfully tracked such transitions in cognitive tasks [12] and neural motor planning [17, 18], effective robotic nudge feedback requires understanding how external interventions influence these transitions. Thus, we employ a probabilistic predictive model of human motor learning using an Input-Output Hidden Markov Model (IOHMM). This structure allows us to causally link specific haptic nudges (inputs) to probabilities of skill improvement, effectively separating execution noise from true latent capability.

Several mechanistic models have been proposed in the literature to explain the doubly stochastic human motor learning process [19–21]. One salient feature of these models is the Markovian evolution of internal/latent states as a function of certain inputs to the model; these models can be discretized to obtain the discrete-time update rule for these latent states. Further binning the continuous latent state space into discrete skill states gives us the standard IOHMM structure. This probabilistic framework allows us to treat the haptic tutoring as a sequential decision problem making under uncertainty. Leveraging the IOHMM, we formulate a Partially Observable Markov Decision Process (POMDP) to derive an optimal nudging policy. Similar to prior work that utilized POMDPs to infer latent user fatigue during rehabilitation [22], our formulation models the evolution of latent motor skill over the duration of the motor task being performed by the learner. The objective is to prescribe a sequence of haptic feedback nudges that minimizes long-term performance cost, implicitly guiding the learner toward effective regions of the latent skill space. This enables a principled, data-driven approach, going beyond performance or expert-designed heuristics, for personalizing haptic feedback design in novel skill acquisition paradigms.

Building on the preliminary findings of our POMDP-based optimal nudge feedback [23], this work investigates the potential of the skill-informed haptic feedback design in accelerating skill acquisition and task performance for high-dimensional, de-novo motor tasks. We distinguish this study from previous work through the following advancements: (i) we introduce another experiment group training on a heuristic-based nudging policy to benchmark performance against the POMDP group, (ii) we increase the sample size to better delineate group effects, (iii) we employ additional analysis to evaluate how effectively different group participants are discovering the task space manifold, (iv) we evaluate the learning dynamics to analyze the learning trajectories and their convergence for the experiment groups, (v) we characterize the participants’ task performance using the reaching error metric, and (vi) we critically discuss the data-driven motor learning behavioral model and provide interpretability to the estimated model parameters. In summary, our contributions are threefold as follows.

1. We introduce a generalizable IOHMM framework that captures the dynamics of high-dimensional motor learning processes as a function of haptic feedback and task difficulty, explicitly decoupling unobservable skill from noisy performance.
2. We formulate a POMDP to compute an optimal, skill-aware haptic nudging policy, providing a principled alternative to heuristic feedback designs.
3. We validate our approach through a human-subject study, demonstrating that our POMDP-derived policy significantly expedites motor skill learning and enhances task performance outcomes compared to both no-feedback baselines and heuristic-based feedback strategies.

The rest of the paper is organized as follows. Section 2 details the experimental setup and theoretical preliminaries. Section 3 describes the behavioral model of human motor learning as an IOHMM in detail. Then, in Section 4, we detail the derived POMDP and design the performance heuristics-based and optimal

nudging policy. Section 5 presents our experimental findings, followed by a discussion of the results and concluding remarks in Section 6.

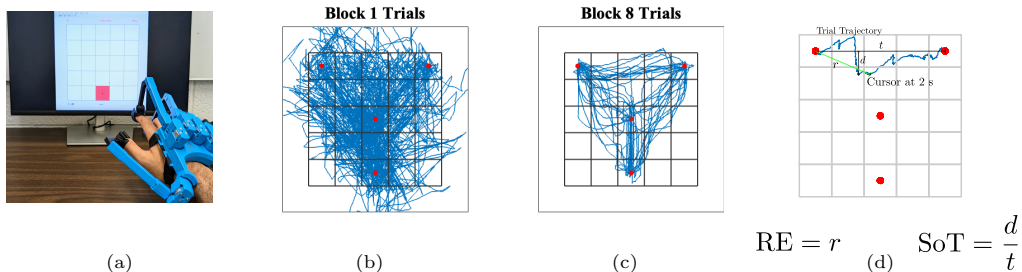


Figure 1: **Target Capture Game:** (a) shows a participant playing our target capture game with the SenseGlove DK1 exoskeleton strapped to their right hand. (b) and (c) show the cursor trajectories during the first and eighth blocks of the game with the red dots representing the target locations. The trajectories get straighter as the participant learns to control the cursor by the end of the experiment session. (d) shows how the performance metrics, Reaching Error and Straightness of Trajectory, are computed.

2 Background

This section details the experimental framework and the performance metrics used to evaluate human performance during the acquisition of a novel, high-dimensional motor skill. Following the experimental description, we outline the stochastic modeling approach, specifically a Markov chain framework employed to characterize how control interventions influence the user’s latent skill state and subsequently modulate observable task performance.

2.1 Experimental Setup

Our study is grounded in the established motor learning principle that the neural mechanisms driving *de-novo* skill acquisition are analogous to those involved in motor recovery following neurological injuries, such as stroke [24]. To operationalize this, we adopt a Body-Machine Interface (BoMI) paradigm similar to those described in [7, 25]. Participants wore a SenseGlove DK1 (manufactured by SenseGlove, a Netherlands-based company), a non-invasive hand exoskeleton capable of tracking 20 distinct degrees of freedom (DoF) across the hand joints. Additionally, the device can deliver independent vibrotactile haptic feedback to each of the five fingertips. This high-dimensional joint space is then projected into a lower-dimensional space, represented by a cursor on a screen. This projection is governed by the linear mapping

$$\dot{\mathbf{x}} = C\mathbf{u}, \tag{1}$$

where $\dot{\mathbf{x}} \in \mathbb{R}^n$ represents the velocity of the screen cursor, $\mathbf{u} = \dot{\mathbf{q}} \in \mathbb{R}^m$ denotes the finger joint velocities derived from the joint angles \mathbf{q} , and $C \in \mathbb{R}^{n \times m}$ serves as the BoMI mapping matrix. In the experimental task, referred to as the *target capture game*¹ (see Fig. 1), participants are instructed to coordinate their finger joint movements to navigate the cursor toward sequentially appearing targets. The targets are prescribed uniformly randomly from a set of 4 targets $\mathcal{T} = \{(0.5, 4.5), (2.5, 2.5), (2.5, 0.5), (4.5, 4.5)\}$ units of the game window grid. Because the mapping from the 20-dimensional hand space to the 2-dimensional cursor space is initially unknown to the user, the task enforces a high-dimensional learning process. Success requires the participant to discover and internalize specific coordinated hand motions consistent with the mapping matrix C . The experimental protocol is the same as that adopted in [23], and we omit it here for brevity.

¹A video footage of the target capture task is available at <https://youtu.be/WIDRwqpE9Sk>

2.2 Performance Metrics

To quantify motor performance, we utilize two primary metrics [21]: **Reaching Error (RE)** and **Straightness of Trajectory (SoT)**, as shown in Fig. 1d.

- RE is defined as the Euclidean distance between the cursor and the target center at the conclusion of a trial. The trial endpoint is determined by the stability condition described above, or a time-out of 2 seconds, whichever occurs first.
- SoT assesses the efficiency of the path. It is calculated as the aspect ratio between the maximum perpendicular deviation of the trajectory from the ideal straight line (connecting the start and end points) and the length of that straight line.

2.3 IOHMM and POMDP Framework

To model the stochastic dynamics of the user’s internal skill-state, we employ an Input-Output Hidden Markov Model (IOHMM) [26]. This probabilistic graphical model describes the evolution of a discrete latent state sequence $\{s_k \in \mathcal{S}\}_{k \in \mathbb{N}}$, where the transition to a future state depends on both the current state s_{k-1} and an exogenous control input or action $a_k \in \mathcal{A}$. Crucially, the true system state is inaccessible for direct measurement; it is hidden. Instead, inference is performed via observable emissions $\{o_k \in \Omega\}_{k \in \mathbb{N}}$. These observations are generated stochastically from the conditional probability distribution $\mathbb{P}(o|s, a)$, representing the likelihood of observing output o given the system is in state s and receives input a . We assume the state space \mathcal{S} and action space \mathcal{A} are finite sets.

The primary objective in training an IOHMM is system identification: estimating the underlying parameters given a historical dataset of input-output pairs $\{a_k, o_k\}_{k \in \mathbb{N}}$. Specifically, we seek to learn the state transition dynamics $T(s, a, s') = \mathbb{P}(s'|s, a)$, the observation probability matrix $O(s, a, o) = \mathbb{P}(o|s, a)$, and the initial state distribution. This parameter estimation is typically achieved via the extended Baum-Welch algorithm [26], which adapts the standard Expectation-Maximization (EM) algorithm to account for the input-dependent structure of the IOHMM.

To transition from system modeling to active control, we extend the IOHMM into a Partially Observable Markov Decision Process (POMDP). The POMDP framework introduces an agent that optimizes the selection of inputs based on a defined objective. Formally, the POMDP is characterized by the tuple $\langle \mathcal{S}, \mathcal{A}, T, R, \Omega, O \rangle$. In this formulation, $\mathcal{S}, \mathcal{A}, T, \Omega$, and O retain their definitions from the IOHMM, while $R(s, a)$ represents the reward function. This function quantifies the agent’s performance goals, assigning positive scalar values to beneficial state-action pairs and penalties (costs) to undesirable outcomes, thereby guiding the optimal control policy.

3 Human Motor Learning Behavioral Model

To develop a behavioral model of the human learners’ response to haptic nudging, we employ a dynamic model of motor performance using an IOHMM. We detail the IOHMM model employed in this work, including its structure and the associated parameters. This is followed by the training/fitting techniques used and the interpretation of this model estimated from the experiment data.

3.1 Behavioral Model

We model the human motor learning behavior as an Input-Output Hidden Markov Model (IOHMM), as illustrated in Fig. 2². The hidden state $h_k \in \{1, \dots, N\}$ represents one of N discrete, latent motor skill states at trial k . To maintain a reasonable number of parameters, the input covariates vector \mathbf{x}_k is composed of two experimental variables: the task complexity, captured by the slope angle u_k of the target pair, and

²The Python package by Mogeng et al. that was used to build and train our IOHMM models can be found at <https://github.com/Mogeng/IOHMM.git>

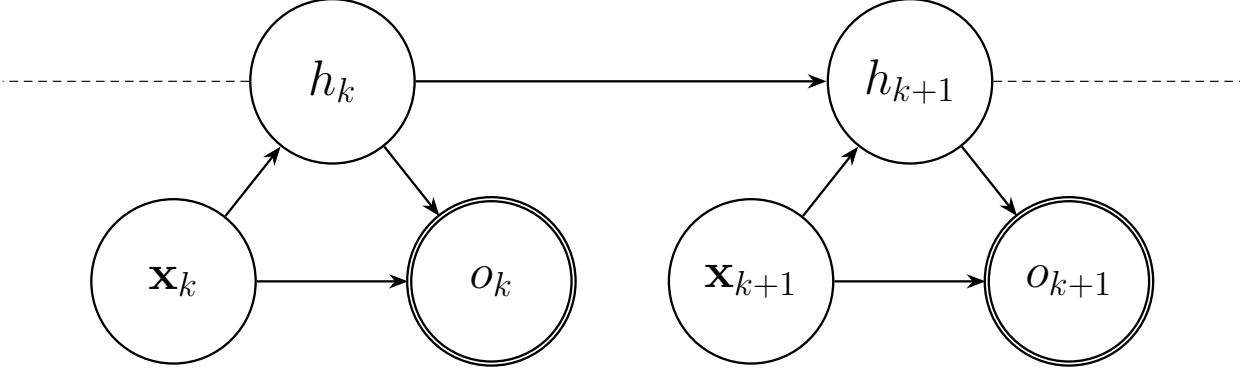


Figure 2: **Simplified IOHMM**: Human motor learning behavior modeled as an IOHMM shows how the hidden motor skill state h_k transitions to h_{k+1} under the effect of the input $\mathbf{x}_k = \{\mathbf{u}_k : \text{slope}_k, \mathbf{a}_k : \text{nudge}_k\}$, leading to the emissions $o_k = \{\text{RE}_k, \text{SoT}_k\}$ under the influence of the same input \mathbf{x}_k .

the haptic guidance, represented by the finger index a_k to which the haptic feedback is applied (an index from 0–5, where 0 denotes no nudge). This prescribed haptic feedback consisted of a tactile stimulus: two sequential vibration bursts, each lasting 150 ms, separated by 2000 ms, delivered to the fingertip indexed a_k . The strength of this nudge is chosen such that it is clearly perceived by the participant, but doesn’t impact the finger motion. A target pair consists of targets for trial k and $k-1$, with their numbering convention following $\{0 : (\mathcal{T}(2), \mathcal{T}(3)), 1 : (\mathcal{T}(1), \mathcal{T}(2)), 2 : (\mathcal{T}(1), \mathcal{T}(3)), 3 : (\mathcal{T}(1), \mathcal{T}(4)), 4 : (\mathcal{T}(2), \mathcal{T}(4)), 5 : (\mathcal{T}(3), \mathcal{T}(4))\}$.

The evolution of the latent motor skill state from trial k to $k+1$ is governed by the transition probability distribution $\mathbb{P}(h_{k+1}|h_k, \mathbf{x}_k)$. The observed emissions (outputs) $\mathbf{o}_k = [\text{RE}_k, \text{SoT}_k]^\top$ represent the performance metrics of the learner: Reaching Error (RE) and Straightness of Trajectory (SoT). The distribution of these outputs is conditional on the current state and the input covariates, defined by the emission models $\mathbb{P}(\mathbf{o}_k|h_k, \mathbf{x}_k)$. Together with the initial state distribution $\mathbb{P}(h_0)$, these components form a predictive model of motor learning behavior under haptic guidance as an IOHMM.

3.2 Estimating the Model Parameters

The parameters of the IOHMM were estimated using the gameplay data collected from the first five participants in the Heuristic Group playing the target capture game with heuristic nudging policy (see Sec. 4.1, and 5.1). Unlike standard HMMs, which utilize fixed probability tables, the IOHMM employs parameterized functions to map the input covariates \mathbf{x}_k to state transitions and emission distributions.

3.2.1 Initial and Transition Models

The initial state distribution $\mathbb{P}(h_0|\mathbf{x}_0)$ and the state transition probabilities $\mathbb{P}(h_{k+1}|h_k, \mathbf{x}_k)$ were modeled using Multinomial Logistic Regression (MNL). Formally, the probability of transitioning from a state $h_k = i$ to a state $h_{k+1} = j$ given input \mathbf{x}_k is defined by the softmax function

$$\mathbb{P}(h_{k+1} = j | h_k = i, \mathbf{x}_k) = \frac{\exp(\mathbf{w}_{ij}^\top \mathbf{x}_k + b_{ij})}{\sum_{l=1}^N \exp(\mathbf{w}_{il}^\top \mathbf{x}_k + b_{il})}, \quad (2)$$

where \mathbf{w}_{ij} and b_{ij} are the coefficient vector and intercept term associated with the transition $i \rightarrow j$. To prevent overfitting given the limited training data, we applied L_2 regularization (Ridge regression) during the fitting process. The initial state distribution follows a randomized initialization since we do not enforce a semantic ordering of the latent states, and only perform a post-hoc re-ordering for visualization and interpretability.

3.2.2 Emission Model

The continuous emission outputs \mathbf{o}_k (comprising RE and SoT) were modeled using a linear Gaussian function. For a given state $h_k = i$, the observation is assumed to be drawn from a multivariate normal distribution where the mean is a linear function of the inputs

$$\mathbb{P}(\mathbf{o}_k \mid h_k = i, \mathbf{x}_k) = \mathcal{N}(\mathbf{o}_k \mid \mathbf{V}_i \mathbf{x}_k + \mathbf{c}_i, \mathbf{\Sigma}_i), \quad (3)$$

where \mathbf{V}_i is the coefficient matrix, \mathbf{c}_i is the intercept vector, and $\mathbf{\Sigma}_i$ is the covariance matrix for state i . The parameters for the emission means were estimated using Ordinary Least Squares (OLS) regression. To enhance model generalization, we applied Elastic-Net regularization, which linearly combines L_1 and L_2 penalties, promoting sparsity while maintaining stability.

3.2.3 Training Algorithm

Since the dependencies in an IOHMM are parametric, the standard Baum-Welch algorithm cannot be applied directly. Instead, we utilized a Generalized Expectation-Maximization (GEM) algorithm. In the Expectation (E) step, the forward-backward algorithm computes the posterior probabilities of being in state i at trial k , denoted $\gamma_k(i)$, and the joint probabilities of transitioning from i to j , denoted $\xi_k(i, j)$. In the Maximization (M) step, rather than counting frequencies, these posterior probabilities serve as sample weights for the supervised learning tasks. The transition parameters (\mathbf{w}, b) are updated by fitting weighted MNL classifiers, and the emission parameters ($\mathbf{V}, \mathbf{c}, \mathbf{\Sigma}$) are updated by fitting weighted linear regressors.

To mitigate the risk of convergence to local optima, we employed a Monte-Carlo (MC) training strategy. We executed multiple training runs, each utilizing one of 5 random permutations of the subject data sequences. From these candidates, the model exhibiting the highest log-likelihood was selected. Empirical analysis on validation datasets confirmed that this permutation-based approach yielded models with superior generalizability compared to a single training sequence.

3.2.4 Model Selection

The model architecture and regularization weights were selected through K-fold cross-validation, maximizing the log-likelihood on validation data. This process yielded an optimal model size of $N = 7$ latent states. The selected hyperparameters were $\alpha_{L_2} = 1.0$ for the transition model, and $\alpha_{en} = 10^{-4}$ with an L_1 -ratio of 0.725 for the emission model.

3.3 State Transition Matrices

To study how the latent skill states probabilistically transition as a function of target pair and nudge feedback, we plot the transition function as state transition matrices for the pair of inputs \mathbf{x}_k . For interpretability, we first order the latent motor skill states from best (0) to worst (6) based on the increasing value of the average of predicted mean(RE) + mean(SoT) out of the emission model (Fig. 3), where the mean(\cdot) is taken over all inputs \mathbf{x}_k . We then analyze these transitions for the hardest and easiest target pair, denoted by their slopes, under the effect of different nudge feedbacks, where 0 refers to no nudge. The order of difficulty of various target pairs is obtained through studying the number of gameplay trials it takes for SoT to converge to a baseline value of 0.3 on average across the five participants whose data is used to estimate the IOHMM. Target pair 0 (see Section 3.1 for target pair numbering convention) with slope $\{\pm 1.57\}$ is the easiest with participants converging to an SoT of 0.3 by trial 19 on average, whereas target pair 2 with slope angle $\{-1.11, 2.03\}$ is the hardest, with SoT converging to 0.3 by trial 210 on average. Fig. 3 shows the state transition matrices corresponding to the target pair 0.

The probabilities show how participants tend to transition from low-performing motor skill states to high-performing motor skill states, ideally imparting an expected (albeit imperfect) lower triangular structure to these matrices owing to the new state ordering.

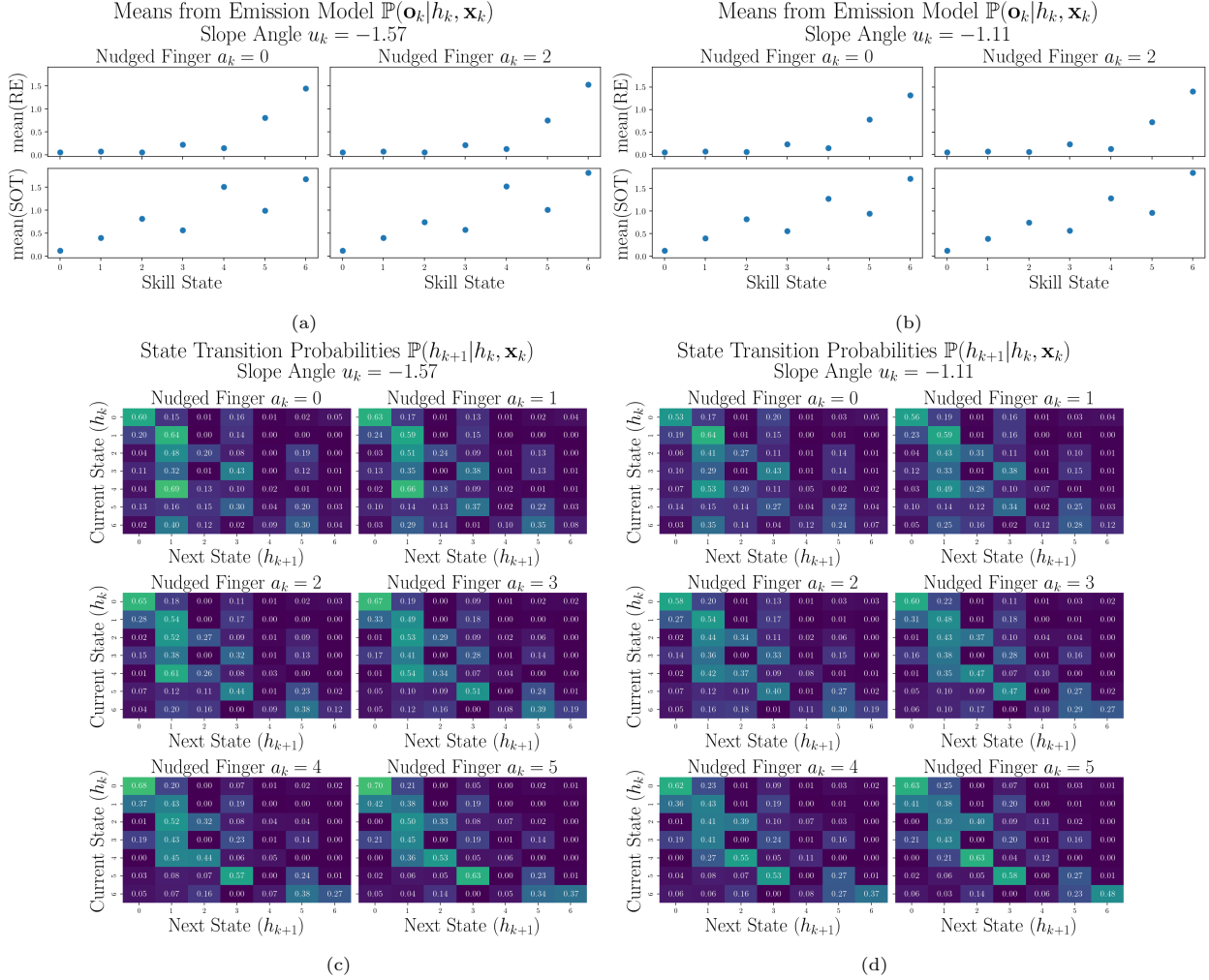


Figure 3: **Estimated Behavioral Model:** (a) Predicted RE and SoT means out of the emission model for the ordered skill states, and (b) State Transition Matrices extracted from the estimated human motor learning behavioral model show how participants tend to transition from low latent skill states to high latent skill states under the effect of the inputs $u_k = -1.57, -1.11$ and $a_k = 0, \dots, 5$. The latent skill states are ordered best-to-worst (0 – 6) based on their mean output RE emission values. The **nudge** = 0 value represents no nudging.

The figure also reveals that for the target pair 0 with slope angle -1.57 , the participants tend to stay in high performing skill states 0, 1 without needing any nudge. Additionally, a nudge to finger 1, which is the thumb, helps them transition from lower to higher performing skill states more prominently. This was also observed in the experiments, where the thumb abduction-adduction majorly led to the screen cursor’s vertical motion. Furthermore, Fig. 3 also shows that for the target pair 2 with slope angle -1.11 , nudges are more helpful for transitioning from lower to higher performing skill states compared to nudges for target pair 0. In both these cases, finger 5, which corresponds to the pinky, had the least effect in transitioning away from lower performing skill states. This is also observed in the experiments, in that the pinky did not contribute much to the cursor motion owing to its relatively lower range of motion.

4 Skill-based Nudging Prescription Design

The application of haptic force feedback offers a promising avenue for expediting motor skill acquisition by providing physical cues that guide the learner toward desired behaviors. Nevertheless, the efficacy of

such interventions in high-dimensional spaces is constrained by two primary obstacles. First, true motor proficiency is a latent variable, an internal state of the neural controller that is inaccessible for direct measurement [27]. Conventional feedback strategies often depend on observable, low-dimensional error metrics as proxies for skill. However, strictly minimizing these kinematic errors does not ensure the development of robust, high-dimensional coordination strategies and may inadvertently reinforce sub-optimal compensatory habits. Second, in contrast to low-dimensional scenarios where reference trajectories are well-defined and can be tracked directly [6, 10], complex high-degree-of-freedom tasks lack a unique “ground truth” trajectory. This redundancy makes it non-trivial to design intuitive feedback that effectively resolves the learner’s kinematic ambiguity. To address these limitations, we propose a paradigm shift from performance-error correction to skill-state-aware guidance. By utilizing the probabilistic model of human motor learning estimated from input-output data (detailed in Section 3), our approach synthesizes personalized haptic nudges. These interventions are designed to regulate the learner’s exploration of the control manifold, thereby fostering the discovery of efficient coordination patterns and accelerating skill learning.

4.1 Heuristic Nudging Policy

To establish a performance baseline, we synthesized a heuristic feedback policy informed by pilot studies. This strategy aims to assist the user by incrementally refining their hand configuration to achieve the current objective. For a specific target t_k presented in trial k , we first calculate a theoretical optimal posture, θ_k^{opt} , by applying the pseudo-inverse of the BoMI mapping matrix, such that $\theta_k^{\text{opt}} = C^\dagger t_k$. We then evaluate the difference between this ideal configuration and the participant’s actual hand posture, θ_k^{curr} , at the onset of the trial. The deviation of each finger i is quantified in joint space as the Sum of Squared Errors (SSE) between the current and optimal angles as

$$d_{i,k} = \sum_{j=1}^4 \left(\theta_{ij,k}^{\text{curr}} - \theta_{ij,k}^{\text{opt}} \right)^2, \quad (4)$$

where $\theta_{ij,k}^{\text{curr}}$ represents the angle of the j^{th} joint of the i^{th} finger at the start of trial k . To prioritize fingers that require minimal adjustment to correct the cursor position, we invert these distance metrics to generate a closeness score. These scores are then normalized into a probability distribution via a `softmax` function with a temperature parameter τ as

$$\mathbb{P}(a_k = i) = \frac{e^{d_{i,k}^{-1}/\tau}}{\sum_{n=1}^5 e^{d_{n,k}^{-1}/\tau}}. \quad (5)$$

The specific finger to receive the haptic nudge is sampled stochastically from this distribution. The underlying logic is that minimizing d_i idempotently identifies the finger capable of producing the most significant cursor position with the least kinematic effort. Consequently, this heuristic functions as a local refinement mechanism. It serves as a computationally lightweight standard against which we evaluate our optimal, POMDP-driven nudging policy.

4.2 POMDP-based Optimal Nudging Policy

To synthesize an active intervention strategy, we recast the predictive IOHMM framework (Section 3) into a control-theoretic POMDP. The primary objective is to compute a policy π that maps a probabilistic belief of the user’s hidden motor state to specific haptic nudge feedback. This policy is optimized to minimize the cumulative expected deviation in performance metrics (RE and SoT) over a long horizon. The POMDP is characterized by the tuple $\langle \mathcal{S}, \mathcal{A}, T, R, \Omega, O \rangle$, with components adapted from the underlying IOHMM structure.

State Space, Action Space, and Observations: We augment the state space to include task-specific context. The POMDP state is defined as the tuple $s_k = (h_k, t_{k-1}, t_k) \in \mathcal{S}$, which encapsulates the latent skill level h_k alongside the previous target t_{k-1} and the current active target $t_k \in \mathcal{T} \setminus \{t_{k-1}\}$. The action

variable $a_k = \text{nudge}_k \in \mathcal{A}$ represents the index of the nudged finger, and the observation space $o_k \in \Omega$ remains consistent with the IOHMM formulation.

Transition and Emission Models: The system dynamics are decomposed into the evolution of the human’s skill and the stochastic progression of the game targets. Given that targets are drawn uniformly randomly (excluding the immediate predecessor) and independent of the motor state, the composite transition model is written as

$$T = \mathbb{P}(s_{k+1}|s_k, a_k) = \mathbb{P}(h_{k+1}|h_k, u_k, a_k) \times \mathbb{P}(t_k). \quad (6)$$

Similarly, the emission model is inherited directly from the IOHMM structure $O = \mathbb{P}(o_k|s_k, a_k) = \mathbb{P}(o_k|h_k, u_k, a_k)$. It is important to note that u_k is deterministically determined from the target pair $\{t_{k-1}, t_k\}$.

Reward Function: To foster both immediate task success and long-term motor learning, the designed reward function $R(s_k, a_k)$ balances instantaneous performance against future skill acquisition potential. Mathematically, this is defined as the negative sum of the expected immediate cost and the generalized utility of the next latent state as

$$R(s_k, a_k) = -(\mathbb{E}[C_{\text{imm}}(s_k, a_k)] + w_g \mathbb{E}[C_{\text{gen}}(h_{k+1}, s_k, a_k)]), \quad (7)$$

where $\mathbb{E}[C_{\text{imm}}(s_k, a_k)]$ denotes the expected cost for the current trial, while $\mathbb{E}[C_{\text{gen}}(h_{k+1}, s_k, a_k)]$ evaluates the expected performance on all possible tasks at the next latent state h_{k+1} . The weighting parameter was fixed at $w_g = 1$. The immediate performance penalty is a linear combination of the predicted means for RE and SoT as

$$\mathbb{E}[C_{\text{imm}}(s_k, a_k)] = \mu_{\text{RE}}(h_k, u_k, a_k) + w_{\text{SoT}} \mu_{\text{SoT}}(h_k, u_k, a_k), \quad (8)$$

where μ_{RE} and μ_{SoT} are the predicted RE and SoT means from the emission model, and $w_{\text{SoT}} = 2$ scales the relative importance of SoT. The expected future utility is calculated by marginalizing over the transition probabilities provided by the IOHMM as

$$\mathbb{E}[C_{\text{gen}}(h_{k+1}, s_k, a_k)] = \sum_{h_{k+1}} \mathbb{P}(h_{k+1}|s_k, a_k) \cdot C_{\text{gen}}(h_{k+1}), \quad (9)$$

where (\cdot) denotes the dot product. The term C_{gen} serves as a pre-computed heuristic for skill versatility. It quantifies the inherent value of latent motor state h_{k+1} by aggregating the expected costs across all possible task conditions (all target transitions and haptic nudges) as

$$C_{\text{gen}} = \sum_{t_{k-1}} \sum_{t_k \neq t_{k-1}} \sum_{a_k} \mathbb{E}[C_{\text{imm}}(s_k, a_k)]. \quad (10)$$

By minimizing this composite cost, the planner is encouraged to select haptic nudge indices that not only reduce current errors but, critically, steer the learner toward skill states with strong performance across all possible tasks.

4.3 Approximate POMDP Solution via QMDP

The state space of the POMDP is characterized by the belief space, a continuous, high-dimensional simplex representing the set of all valid probability distributions over the underlying POMDP states $s_k \in \mathcal{S}$. Given the computational intractability of applying standard infinite-horizon value iteration directly to this continuous space, we adopt the QMDP approximation method [28]. This algorithm computes $Q_{MDP}(s, a)$ values for the underlying MDP by utilizing only the transition and reward models, effectively bypassing the observation model to render the problem tractable. Although this approach technically assumes full state observability, an assumption that does not hold in our partial information setting, it yields a robust policy π^* that can be applied to states sampled from the current belief distribution. To further robustify the policy against model imperfections stemming from limited training data, the MDP is solved via infinite-horizon soft-value iteration.

The value update rule follows the soft Bellman optimality equation $V(s) \leftarrow \alpha \log \sum_{a \in \mathcal{A}} \exp\left(\frac{Q(s,a)}{\alpha}\right)$, where α denotes the temperature parameter. The corresponding action-value function $Q(s, a)$ is defined as

$$Q(s_k, a_k) = R(s_k, a_k) + \gamma \sum_{s_{k+1} \in \mathcal{S}} \mathbb{P}(s_{k+1}|s_k, a_k) V(s_{k+1}). \quad (11)$$

The algorithm iterates until the value function $V(s_k)$ converges across the state space. The final output is a stochastic policy $\pi(a|s_k)$, formulated as a softmax distribution over the Q -values, which assigns a selection probability to each haptic nudge prescription. For this implementation, we used $\alpha = 0.2$ and $\gamma = 0.98$.

Real-Time Policy Execution and Belief Update

The derived stationary policy is integrated into the experiment for real-time execution. Throughout the experiment, the system maintains a running belief state $b_k := b(s_k)$, representing the posterior probability distribution $\mathbb{P}(s_k|o_k, a_k, s_{k-1})$. The selection of the specific finger index for haptic feedback proceeds in two stages: first, a state hypothesis s_k is sampled from the current belief distribution $s_k \sim b_k$; second, the action a_k is sampled from the policy distribution $\pi^*(a|s_k)$ corresponding to that sampled state. Following the prescription of the haptic nudge by the BoMI, the system records the participant’s trial performance metrics $o_k = \{\mathbf{RE}_k, \mathbf{SoT}_k\}$. The belief state is then advanced to the subsequent time step via the Bayesian filter

$$b_{k+1} = \eta \mathbb{P}(o_k|s_k, a_k) \sum_{s \in \mathcal{S}} \mathbb{P}(s_{k+1}|s_k, a_k) b_k, \quad (12)$$

where η is the normalization constant. This updated belief b_{k+1} encapsulates the new system knowledge and is used in the decision process for the next trial.

5 Results

This section presents the findings from our human-subject study, designed to test the hypothesis that haptic feedback informed by the learner’s latent skill state accelerates motor acquisition and enhances task performance relative to both a no-feedback baseline and a standard heuristics-based strategy.

5.1 Experiment Details

To validate our approach, we divided participants into three distinct experimental groups, all of whom performed the target capture task described in Section 2.1. These groups were defined as follows: a Control Group, which received no haptic feedback; a Heuristics Group, which received feedback based on a heuristics-based nudge feedback policy; and a POMDP Group, which received feedback derived from our optimal, skill-state-aware policy. Each group consisted of 10 participants³. The experimental timeline was structured sequentially. First, data was collected from the Heuristics Group. The input-output gameplay data from the initial five participants in this group were utilized to train the Input-Output Hidden Markov Model (IOHMM), establishing the baseline behavioral model of human motor learning. For the POMDP Group, the haptic feedback was generated by casting the problem as a POMDP and solving it approximately via the QMDP method. During the experiment, the system maintained a running belief state, which was updated after every trial. To select an optimal action for the subsequent trial, a state was sampled from this current belief distribution and mapped to a specific nudge finger index via the QMDP policy. The belief state was initialized using the prior distribution $\mathbb{P}(h_0)$ derived from the trained IOHMM.

³All human subject experiments were approved under the Michigan State University Institutional Review Board Study ID LEGACY14-431M.

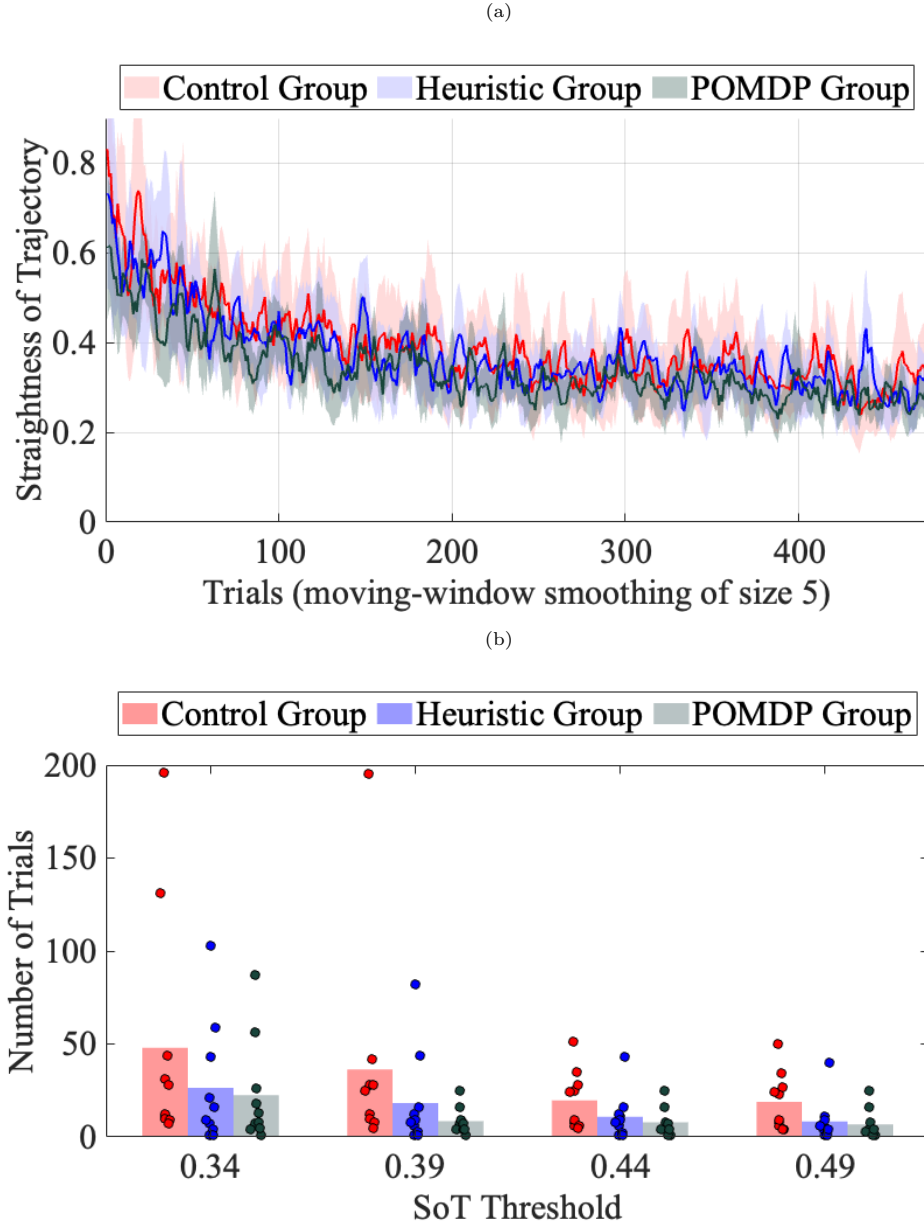


Figure 4: **Task Performance:** (a) Mean SoT curves (with 95% confidence intervals) of the three group participants, and (b) the mean number of trials (along with the scatter plot taken across participants) to converge to a specific SoT threshold under the three nudging policies shows fastest convergence for participants trained on POMDP-based optimal nudging policy, followed by the heuristic policy. The low p-values from two-tailed tests from the linear mixed model fits show a decrease in SoT across trials and in the number of trials required by the POMDP group for various SoT thresholds. Each scatter plot point represents the number of trials taken by a participant to achieve the SoT threshold.

5.2 Task Performance: Straightness of Trajectory

We used the Straightness of Trajectory SoT to measure task performance across the three groups, where a lower value signifies a smoother, more desirable movement. We conducted two primary analyses to compare the three participant groups. First, we tracked the evolution of SoT across all game trials to assess the overall performance trajectories. Second, we computed the number of trials required for participants to converge to a predefined SoT threshold. This convergence analysis directly evaluates the efficiency of a nudging policy, as

haptic feedback can nudge participants towards efficient joint motions that could improve task performance and thus require fewer trials to reach a performance threshold. Moreover, a nudging policy based on the motor skill state of the participant could help achieve accelerated motor skill acquisition by optimally nudging the right joints towards better synergistic patterns, going beyond simple task performance improvements. To analyze performance across the full learning trajectory, we fit a Linear Mixed Model (LMM) to the SoT values for all 480 gameplay trials from each participant, with trial number, group, and their interaction as fixed effects, and a random intercept per participant, estimated via Restricted Maximum Likelihood (REML) [29]. This model accounts for the correlation structure arising from repeated measurements within participants. Post-hoc two-tailed contrasts with Bonferroni correction were used to test for pairwise differences between the POMDP, heuristic, and control groups. For the threshold-based analysis, where each participant contributes a single scalar value (the trial index at which a given SoT threshold is first reached), we conducted a one-way ANOVA to test for an overall group effect, followed by pairwise independent-samples t-tests (two-tailed) with Bonferroni correction.

The results from Fig. 4 show that SoT decreases with trials for all groups, and the mean number of trials taken to achieve a particular SoT threshold also decreases for increasing thresholds, indicating task learning improvement through training. The p-values from Table 1 show that participants trained on the optimal nudging policy differ statistically significantly (at a significance level of $\alpha = 0.10$) in average SoT convergence across the game trials as compared to participants trained without any haptic feedback. On average, the POMDP group takes fewer trials than the control group to converge to different SoT thresholds. This indicates expedited performance improvement in the early stages of training. Fig. 4 shows that the POMDP group takes fewer trials to hit SoT thresholds compared to the heuristic group, and has faster SoT convergence throughout the game trials; however, the results are not statistically significant.

5.3 Motor Output Performance: Reaching Error

We used the reaching error RE to measure the motor output performance for the three experiment groups. Recall that the RE for a game trial is the Euclidean distance of the screen cursor from the trial target at the end of 2 s, or end of movement, whichever is earlier. Thus, lower RE values signify better motor output and task learning. We performed two analyses: first, we studied the evolution of RE across gameplay trials to assess overall motor performance, and second, we tracked the number of trials required for participants to converge to predefined RE thresholds. The statistical analyses employed here are the same as in Section 5.2.

Results from Fig. 5 show that the RE decreases across all groups as the gameplay progresses, indicating improved motor performance with training. The POMDP group achieves statistically significantly (at significance level $\alpha < 0.10$) lower RE compared to the other two groups across all gameplay trials, as shown in Table 2. Results also show that the POMDP group requires fewer trials on average to converge to lower RE thresholds (Fig. 5b) than the control and the heuristic group, indicating expedited motor performance improvement; however, the results are not statistically significant.

Table 1: **Two-tailed Contrasts for SoT Group Differences.** The p-values for the hypothesis that the POMDP group has different SoT values across gameplay trials and different number of trials to achieve thresholds compared to the control and the heuristic group are reported. The results show that the POMDP group achieves lower SoT values on average, and takes statistically significantly (at significance level $\alpha = 0.10$) fewer gameplay trials to achieve SoT thresholds early in the training.

| Metrics | | POMDP vs Control | | POMDP vs Heuristic | |
|----------------|------|-------------------|--------------------|--------------------|--------------------|
| | | p_{bonf} | d_{cohen} | p_{bonf} | d_{cohen} |
| SoT Curve | | 0.1053 | -0.5368 | 0.5002 | -0.6048 |
| SoT Thresholds | 0.34 | 0.5290 | -0.5151 | 1.0000 | -0.1277 |
| | 0.39 | 0.2865 | -0.6845 | 1.0000 | -0.5148 |
| | 0.44 | 0.0875 | -0.9698 | 1.0000 | -0.2950 |
| | 0.49 | 0.0796 | -0.9912 | 1.0000 | -0.1619 |

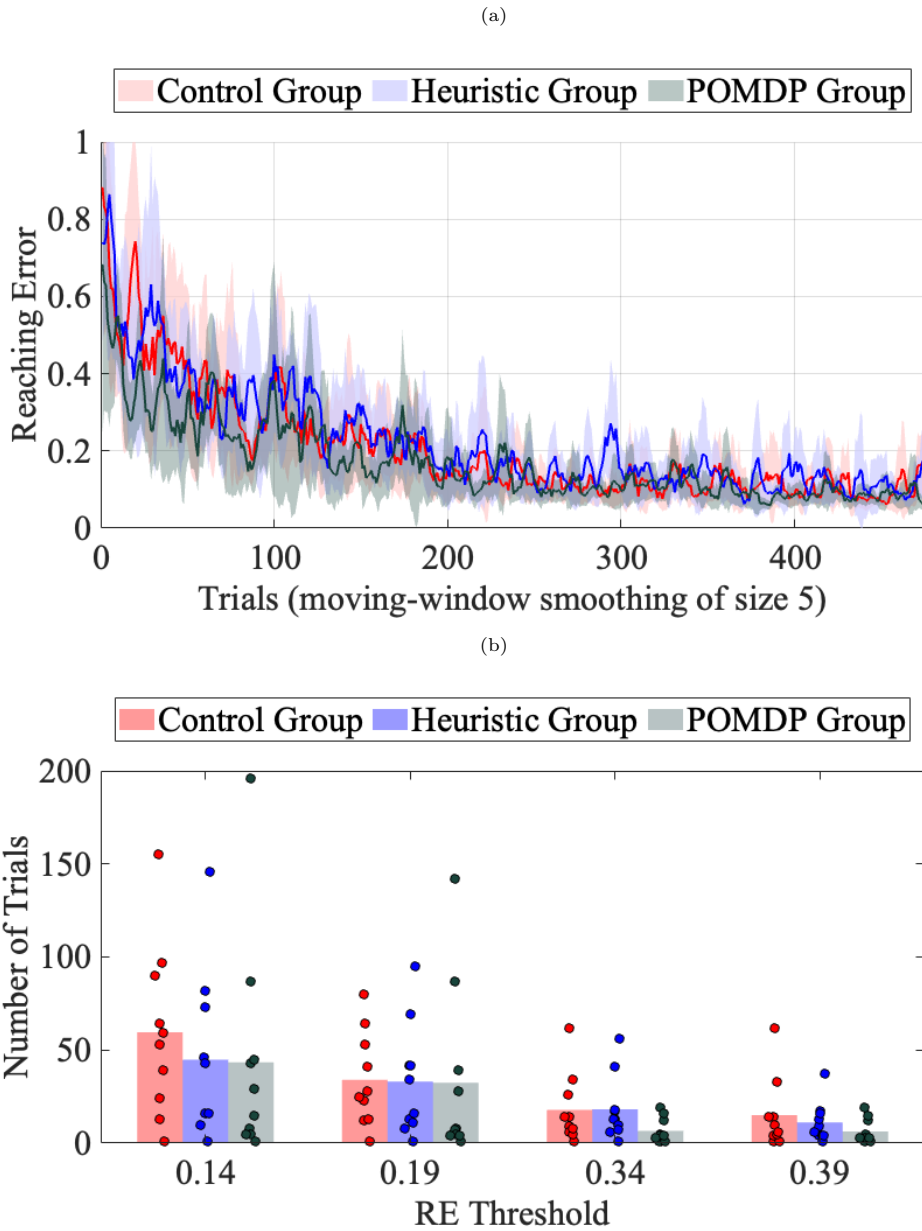


Figure 5: **Motor Output Performance:** (a) Mean RE curves (with 95% confidence intervals) of the three group participants, and (b) the mean number of trials (along with the scatter plot taken across participants) to converge to different RE thresholds under the three nudging policies shows fastest convergence for participants trained on POMDP-based optimal nudging policy. The low two-tailed test p-values from the linear mixed model fits show a decrease in RE across trials and in the number of trials required by the POMDP group for all RE thresholds. Each scatter plot point represents the number of trials taken by a participant to achieve that RE threshold.

5.4 Synergy Analysis

The inherent high redundancy in the target capture game requires participants to identify an underlying manifold to effectively map finger joint movements to desired cursor motion towards the targets. To characterize how coordination strategies emerge, we analyzed the simplification of motor-control dimensionality across the three groups by calculating the Variance Accounted For (VAF) by the first few Principal Components (PCs) derived from the hand postures data (finger joint angles \mathbf{q}). For this analysis, the eight training blocks were condensed into four phases (two blocks per phase) for ease of representation. We also

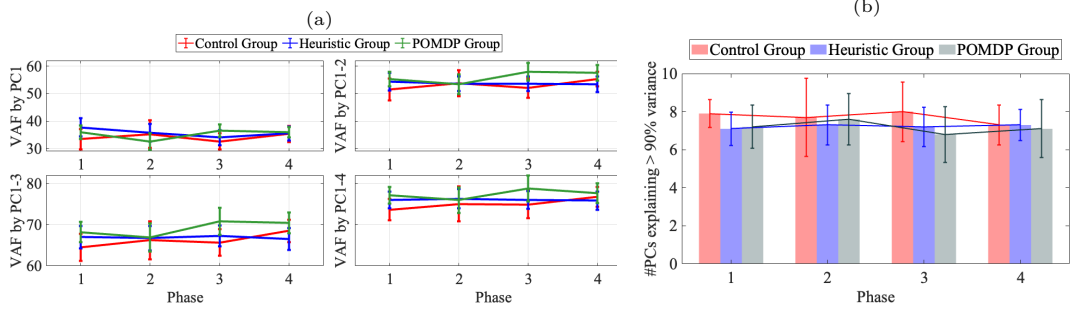


Figure 6: **Synergy Analysis:** (a) Variance accounted for (VAF) by the first four principal components (PC), and (b) the number of PCs required to explain more than 90% variance in joint data across the three participant groups reveal that the POMDP group achieved a higher VAF by top-PCs (especially in later phases) and required fewer PCs to explain > 90% variance in the data on average, signifying a more rapid discovery of the task relevant subspace towards expedited skill acquisition. Training blocks are consolidated into phases, with each phase consisting of two consecutive blocks.

analyze the number of PCs required to explain more than 90% variance in the data across the three groups. We hypothesized that the POMDP group would exhibit a faster increase in top-PC VAF, indicating more efficient discovery of the 2D task-relevant subspace.

Group Comparison: As illustrated in Fig. 6, the POMDP group achieved higher average VAF in the first four PCs, particularly in later training phases, and required fewer PCs on average to explain > 90% of the variance in joint angle data. These results provide a structural explanation for the POMDP group’s improved task learning and motor output performance. By discovering the task space more rapidly than other groups, POMDP group participants successfully coordinated their 20 finger joints into a simpler, more effective strategy, which is a direct indication of accelerated skill acquisition driven by the optimal nudge feedback.

5.5 Learning Dynamics and Convergence Analysis

To quantify the temporal dynamics of motor learning beyond simple performance metrics, we analyzed the evolution of the participants’ latent states throughout the experiment. While the IOHMM provides a discrete set of hidden states representing different performance strategies, the POMDP framework maintains a continuous belief state $b_k \in \mathbb{R}^7$ representing the probability distribution over these states at trial k . This probabilistic approach allows us to capture the uncertainty and the transitional phases of learning that discrete classification might miss.

Expected Latent State: The state ordering obtained in Section 3.3 is preserved in this analysis, with state 0 as the best and state 6 as the worst performing. To visualize the learning trajectory, we computed

Table 2: **Two-tailed Contrasts for RE Group Differences.** The p-values for the hypothesis that the POMDP group has different RE values across gameplay trials and different number of trials to achieve thresholds compared to the control and the heuristic group are reported. The results show that the POMDP group achieves statistically significantly (at significance level $\alpha = 0.10$) lower RE values on average, and takes fewer gameplay trials to achieve RE thresholds early in the training.

| Metrics | POMDP vs Control | | POMDP vs Heuristic | |
|----------------------|-------------------|--------------------|--------------------|--------------------|
| | p_{bonf} | d_{cohen} | p_{bonf} | d_{cohen} |
| RE Curve | 0.0642 | -0.3863 | 0.0249 | -0.5899 |
| RE Thresholds | 0.14 | 1.0000 | 1.0000 | -0.0284 |
| | 0.19 | 1.0000 | 1.0000 | -0.0153 |
| | 0.34 | 0.1705 | 0.1223 | -0.8932 |
| | 0.39 | 0.3765 | 0.4802 | -0.5433 |

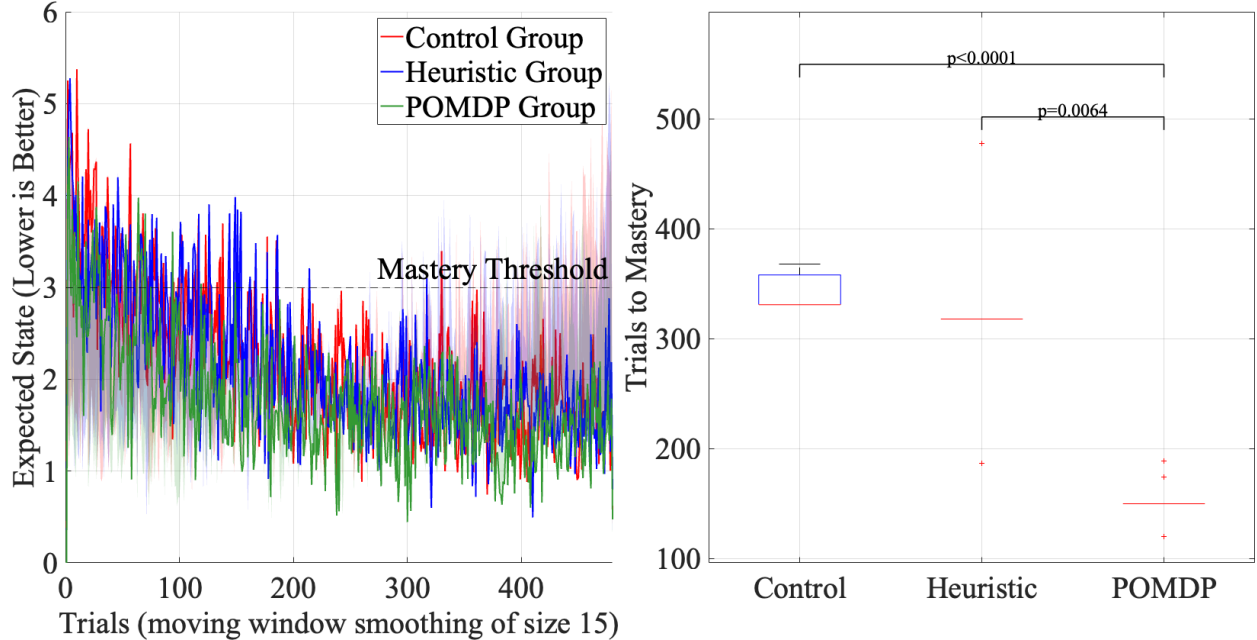


Figure 7: **Learning Dynamics and Convergence Analysis:** Expected latent state evolution across trials and the number of trials to reach a steady state mastery level ($\mathbb{E}[s_k] < 3$) reveals expedited convergence of POMDP group to better performing states and a statistically significantly lower number of trials to mastery, compared to heuristic and control groups.

the *Expected Latent State* for each trial, defined as the probability-weighted average of the state ranks as

$$\mathbb{E}[s_k] = \sum_{i=0}^6 i \cdot b_k(i) \quad (13)$$

where $b_k(i)$ is the belief (probability) that the participant is in the i -th ranked state at trial k . A value of $\mathbb{E}[s_k]$ closer to 0 indicates a high probability of having adopted an optimal control strategy.

Convergence Results: Figure 7 illustrates the average Expected State trajectories for the three experimental groups over the course of the 480 trials. Shaded regions indicate the standard error of the mean. All groups exhibited a characteristic learning curve, initiating the experiment with an Expected State around 5, indicating initial exploratory behavior and high motor error. As the experiment progressed, a monotonic mean decrease in $\mathbb{E}[s_k]$ was observed, reflecting the acquisition of the BoMI mapping C .

Group Comparison: The POMDP group demonstrated an expedited rate of convergence compared to the other two groups. Specifically, the POMDP group reached a steady-state mastery level (defined as $\mathbb{E}[s_k] < 3$) by trial 150 (median), whereas the control and the heuristic groups reached this threshold statistically significantly later ($p < 0.0001$ for $\text{Trials}(\text{POMDP}) < \text{Trials}(\text{Control})$, and $p = 0.0064$ for $\text{Trials}(\text{POMDP}) < \text{Trials}(\text{Heuristic})$). This suggests that the optimal nudging policy effectively guided participants away from suboptimal local minima and facilitated a more rapid transition into high-performance states. The lower entropy in the belief distribution for the POMDP group towards the end of the session further indicates that these participants not only performed better but had settled into a more stable and confident control strategy compared to other groups. Since the trials to reach this threshold were not normally distributed across the group participants, we used the Kruskal-Wallis test for statistical significance (at significance level $\alpha < 0.05$). This was followed by post-hoc one-tailed contrasts to compare the POMDP group with the other two groups.

6 Discussion

This work proposes a POMDP-based framework for expediting complex motor skill acquisition and task performance using skill-state-based optimal haptic feedback policy. This proposed approach shows accelerated task performance compared to no feedback, and a performance heuristics-based feedback design by leveraging the learner’s estimated motor skill state. These promising results underscore the significant potential of skill-informed haptic feedback in improving the motor learning process and the corresponding task performance, particularly in novel complex motor skill acquisition tasks.

6.1 Decoupling Latent Skill from Observable Performance

A central pillar of our approach is the distinction between task/motor performance and latent skill acquisition. Our results demonstrate that nudge feedback policies targeting observable performance metrics (Heuristic Group) do not necessarily lead to superior learning and performance outcomes compared to no-feedback baselines (Control Group). This aligns with the ‘Guidance Hypothesis’ in motor learning literature [30], which suggests that outcome-based error-correction can engender dependency, allowing the learner to perform well during training without internalizing the task dynamics.

In contrast, the POMDP-based optimal nudging policy effectively decoupled execution noise from the underlying true skill through the estimated behavioral model of motor learning. By optimizing for long-term state transitions (C_{gen}) rather than immediate motor performance (C_{imm}), the optimal policy likely permitted short-term performance deviations if they facilitated exploration of the state space. This supports the notion that effective robotic tutoring should operate as an active teacher, prioritizing the resolution of internal model inaccuracies/uncertainties over instantaneous kinematic error corrections. The statistical superiority of the POMDP group in both RE and SoT performance and convergence (Tables 1 and 2) validates the utility of modeling learning as evolution through discrete latent states rather than a continuous improvement in task performance.

6.2 Accelerated Discovery of Better Task Manifolds

High-dimensional *de-novo* tasks require learners to solve the redundancy problem: idempotizing a low-dimensional subspace (manifold) within the high-dimensional task space that maps effectively to the task goal. Our synergy analysis (Fig. 6) reveals that the POMDP group exhibited a more rapid consolidation of joint space variance into the first few PCs compared to the other two groups.

This suggests that the skill-state aware nudge feedback did not merely improve task performance, but actively guided participants toward the discovery of the better task manifolds. This behavior is also supported by the learning dynamics and convergence analysis results in Fig. 7. Critically, by penalizing the transition to low-performing skill states, the POMDP policy likely encouraged the utilization of correct fingers sequentially to foster coordinated joint movement strategies toward expedited skill acquisition. This finding is consistent with the Uncontrolled Manifold (UCM) hypothesis, suggesting that optimal assistance facilitates the separation of task-relevant and task-irrelevant variabilities, facilitating the discovery and utilization of effective synergies.

6.3 Interpretability of Data-driven Behavior Models

While data-driven models are often criticized for their lack of interpretability (black-box models) compared to mechanistic first-principle models, our IOHMM successfully captured biomechanically relevant features of the task. The state transition matrices in Fig. 3 revealed that the haptic nudges to the thumb (finger index 1) significantly increased the probability of transitioning to higher skill states, whereas nudges to the pinky (finger index 5) had a smaller impact. Furthermore, the STMs for neighboring nudged fingers are closer to each other than the rest.

This aligns with the kinematic realities of our setup and the BoMI, where the thumb possesses a larger range of motion and greater contribution to cursor motions than the other fingers. The model learned these

biomechanical constraints solely from the input-output data, without explicit biomechanical modeling. This validates the IOHMM not just as a control tool, but as a diagnostic tool capable of identifying which fingers are most receptive to haptic interventions at specific stages of learning. Such interpretability is crucial for clinical application, where therapists must trust the agent to prescribe physiologically valid movement patterns.

6.4 Limitations and Future Directions

While our results are promising, several limitations warrant discussion. First, the discretization of skill state into $N = 7$ states is an abstraction of the continuous motor learning process. While necessary for the tractability of the QMDP solver, this quantization may mask subtle changes/adjustments in a strategy that occur within a single state. Future work could explore continuous state POMDP solvers or hybrid approaches to capture the finer details/granularities in the learning dynamics.

Second, our study validated the proposed framework on healthy humans learning a novel motor task. While this paradigm is an established proxy for the motor re-learning process, post neurological injury populations introduce state-dependent constraints owing to specific impairments (eg, spasticity, paresis) that are not modeled in healthy participants. However, the data-driven nature of our IOHMM framework is agnostic to specific learning dynamics. In principle, the same pipeline could be applied to patient data to learn the personalized transition model; however, this would necessitate the use of individualized models instead of a population-average model. Another possibility is to estimate a population average model, personalizing it to each individual using real-time input-output data during the gameplay. Future efforts could focus on transitioning this framework to clinical cohorts to validate its efficacy in neuro-rehabilitation.

References

- [1] L. Marchal-Crespo and D. J. Reinkensmeyer, “Review of control strategies for robotic movement training after neurologic injury,” *Journal of Neuroengineering and Rehabilitation*, vol. 6, no. 1, p. 20, 2009.
- [2] C. K. Williams and H. Carnahan, “Motor learning perspectives on haptic training for the upper extremities,” *IEEE Transactions on Haptics*, vol. 7, no. 2, pp. 240–250, 2014.
- [3] D. M. Wolpert, J. Diedrichsen, and J. R. Flanagan, “Principles of sensorimotor learning,” *Nature Reviews Neuroscience*, vol. 12, no. 12, p. 739, 2011.
- [4] A. Turolla, O. A. Daud Albasini, R. Oboe, M. Agostini, P. Tonin, S. Paolucci, G. Sandrini, A. Venneri, and L. Piron, “Haptic-based neurorehabilitation in poststroke patients: A feasibility prospective multicentre trial for robotics hand rehabilitation,” *Computational and Mathematical Methods in Medicine*, vol. 2013, no. 1, p. 895492, 2013.
- [5] C.-Y. Lin, C.-M. Tsai, P.-C. Shih, and H.-C. Wu, “Development of a novel haptic glove for improving finger dexterity in poststroke rehabilitation,” *Technology and Health Care*, vol. 24, no. 1_suppl, pp. S97–S103, 2016.
- [6] P. Esmatloo and A. D. Deshpande, “Fingertip position and force control for dexterous manipulation through model-based control of hand-exoskeleton-environment,” in *2020 IEEE/ASME International Conference on Advanced Intelligent Mechatronics (AIM)*. IEEE, 2020, pp. 994–1001.
- [7] R. Ranganathan, A. Adewuyi, and F. A. Mussa-Ivaldi, “Learning to be lazy: Exploiting redundancy in a novel task to minimize movement-related effort,” *Journal of Neuroscience*, vol. 33, no. 7, pp. 2754–2760, 2013.
- [8] E. Basalp, P. Wolf, and L. Marchal-Crespo, “Haptic training: which types facilitate (re) learning of which motor task and for whom? answers by a review,” *IEEE Transactions on Haptics*, vol. 14, no. 4, pp. 722–739, 2021.

- [9] R. Sigrist, G. Rauter, R. Riener, and P. Wolf, “Augmented visual, auditory, haptic, and multimodal feedback in motor learning: A review,” *Psychonomic Bulletin & Review*, vol. 20, no. 1, pp. 21–53, 2013.
- [10] J. L. Sullivan, S. Pandey, M. D. Byrne, and M. K. O’Malley, “Haptic feedback based on movement smoothness improves performance in a perceptual-motor task,” *IEEE Transactions on Haptics*, vol. 15, no. 2, pp. 382–391, 2021.
- [11] J. B. Rowe, V. Chan, M. L. Ingemanson, S. C. Cramer, E. T. Wolbrecht, and D. J. Reinkensmeyer, “Robotic assistance for training finger movement using a hebbian model: a randomized controlled trial,” *Neurorehabilitation and Neural Repair*, vol. 31, no. 8, pp. 769–780, 2017.
- [12] C. Tenison and J. R. Anderson, “Modeling the distinct phases of skill acquisition.” *Journal of Experimental Psychology: Learning, Memory, and Cognition*, vol. 42, no. 5, p. 749, 2016.
- [13] J. Yang, Y. Xu, and C. S. Chen, “Hidden markov model approach to skill learning and its application to telerobotics,” *IEEE Transactions on Robotics and Automation*, vol. 10, no. 5, pp. 621–631, 1994.
- [14] S. Zhang and H.-H. Chang, “A multilevel logistic hidden markov model for learning under cognitive diagnosis,” *Behavior Research Methods*, vol. 52, no. 1, pp. 408–421, 2020.
- [15] S. Wang, Y. Yang, S. A. Culpepper, and J. A. Douglas, “Tracking skill acquisition with cognitive diagnosis models: A higher-order, hidden markov model with covariates,” *Journal of Educational and Behavioral Statistics*, vol. 43, no. 1, pp. 57–87, 2018.
- [16] P. M. Fitts and M. I. Posner, “Human performance,” 1967.
- [17] C. Kemere, G. Santhanam, B. M. Yu, A. Afshar, S. I. Ryu, T. H. Meng, and K. V. Shenoy, “Detecting neural-state transitions using hidden markov models for motor cortical prostheses,” *Journal of Neurophysiology*, vol. 100, no. 4, pp. 2441–2452, 2008.
- [18] S. Kirzherr, S. Mildiner Moraga, G. Coudé, M. Bimbi, P. F. Ferrari, E. Aarts, and J. J. Bonaiuto, “Bayesian multilevel hidden markov models identify stable state dynamics in longitudinal recordings from macaque primary motor cortex,” *European Journal of Neuroscience*, vol. 58, no. 3, pp. 2787–2806, 2023.
- [19] M. A. Smith, A. Ghazizadeh, and R. Shadmehr, “Interacting adaptive processes with different timescales underlie short-term motor learning,” *PLoS Biology*, vol. 4, no. 6, p. e179, 2006.
- [20] C. Pierella, M. Casadio, F. A. Mussa-Ivaldi, and S. A. Solla, “The dynamics of motor learning through the formation of internal models,” *PLoS Computational Biology*, vol. 15, no. 12, p. e1007118, 2019.
- [21] A. Kamboj, R. Ranganathan, X. Tan, and V. Srivastava, “Human motor learning dynamics in high-dimensional tasks,” *PLOS Computational Biology*, vol. 20, no. 10, p. e1012455, 2024.
- [22] R. Huq, P. Kan, R. Goetschalckx, D. Hébert, J. Hoey, and A. Mihailidis, “A decision-theoretic approach in the design of an adaptive upper-limb stroke rehabilitation robot,” in *2011 IEEE International Conference on Rehabilitation Robotics*. IEEE, 2011, pp. 1–8.
- [23] A. Kamboj, R. Ranganathan, X. Tan, and V. Srivastava, “Toward skill-informed haptic feedback for human motor learning in high-dimensional de-novo tasks,” in *American Control Conference*, New Orleans, LA, 2026, accepted for publication.
- [24] J. W. Krakauer, “Motor learning: its relevance to stroke recovery and neurorehabilitation,” *Current Opinion in Neurology*, vol. 19, no. 1, pp. 84–90, 2006.
- [25] K. M. Mosier, R. A. Scheidt, S. Acosta, and F. A. Mussa-Ivaldi, “Remapping hand movements in a novel geometrical environment,” *Journal of Neurophysiology*, vol. 94, no. 6, pp. 4362–4372, 2005.

- [26] Y. Bengio and P. Frasconi, “Input-output HMMs for sequence processing,” *IEEE Transactions on Neural Networks*, vol. 7, no. 5, pp. 1231–1249, 1996.
- [27] R. A. Schmidt, T. D. Lee, C. Winstein, G. Wulf, and H. N. Zelaznik, *Motor Control and Learning: A Behavioral Emphasis*. Human Kinetics, 2018.
- [28] M. L. Littman, A. R. Cassandra, and L. P. Kaelbling, “Learning policies for partially observable environments: Scaling up,” in *Machine Learning Proceedings 1995*. Elsevier, 1995, pp. 362–370.
- [29] R. R. Corbeil and S. R. Searle, “Restricted maximum likelihood (REML) estimation of variance components in the mixed model,” *Technometrics*, vol. 18, no. 1, pp. 31–38, 1976.
- [30] T. D. Lee, M. A. White, and H. Carnahan, “On the role of knowledge of results in motor learning: Exploring the guidance hypothesis,” *Journal of Motor Behavior*, vol. 22, no. 2, pp. 191–208, 1990.